The steady-state distribution of gating charge in crayfish giant axons

Marine Biological Laboratory
LIBRARY
JAN 20 1989
Woods Hole, Mass.

Martin D. Rayner and John G. Starkus
Department of Physiology, John A. Burns School of Medicine, and the Békésy Laboratory of Neurobiology, Pacific Biomedical Research Center, University of Hawaii, Honolulu, Hawaii 96822

ABSTRACT Progressive shifts of holding potential (V_h) in crayfish giant axons, from −140 to −70 mV, reduce gating currents seen in depolarizing steps (to 0 mV test potential) while proportionately increasing gating currents in hyperpolarizing steps (to −240 mV). The resulting sigmoid equilibrium charge distribution (Q-V_h curve) shows an effective valence of 1.9e and a midpoint of −100 mV. By contrast, Q-V curves obtained using hyperpolarizing and/or depolarizing steps from a single holding potential, change their "shape" depending on the chosen holding potential. For holding potentials at the negative end of the Q-V_h distribution (e.g., −140 mV), negligible charge moves in hyperpolarizing pulses and the Q-V curve can be characterized entirely from depolarizing voltage steps. The slope of the resulting simple sigmoid Q-V curve also indicates an effective valence of 1.9e. When the axon is held at less negative potentials significant charge moves in hyperpolarizing voltage steps. The component of the Q-V curve collected using hyperpolarizing pulses shows a significantly reduced slope (~0.75e) by comparison with the 1.9e slope found using depolarizing pulses or from the Q-V_h curve. As holding potential is shifted in the depolarizing direction along the Q-V_h curve, an increasing fraction of total charge movement must be assessed in hyperpolarizing voltage steps. Thus charge moving in the low slope component of the Q-V curve increases as holding potential is depolarized, while charge moving with high apparent valence decreases proportionately. Additional results, together with simulations based on a simple kinetic model, suggest that the reduced apparent valence of the low slope component of the Q-V curve results from gating charge immobilization occurring at holding potential. Immobilization selectively retards that fraction of total charge moving in hyperpolarizing pulses. Misleading conclusions, as to the number and valence of the gating particles, may therefore be derived from Q-V curves obtained by other than depolarizing pulses from negative saturated holding potentials.

INTRODUCTION

Both Keynes and Rojas (1974) and Meves (1974) recognized that the increase in gating charge movement (Q) with change in test potential (V) should indicate the voltage sensitivity of the sodium channel gating particles. The Q-V curves they obtained appeared well fitted by either a Boltzmann distribution with an effective valence of 1.3e (Fig. 19 in Keynes and Rojas, 1974) or by the Langevin-Debye function with a dipole moment of 840 Debye units (Fig. 3 in Meves, 1974). The symmetrical sigmoid shape of the Q-V curves seen in these early studies is particularly well exemplified by the data of Keynes and Rojas (1976), indicating a valence of 1.3e and a midpoint of −26 mV, for squid axons from a holding potential of −100 mV. However more recent studies have raised two issues which complicate the interpretation of Q-V curves.

Address correspondence to Dr. Martin D. Rayner, University of Hawaii, Pacific Biomedical Research Center, Békésy Laboratory of Neurobiology, 1993 East West Road, Honolulu, HI 96822. INTERNET: Martin@uhccux.uhcc.hawaii.edu. BITNET: Martin@uhccux.

First, the Q-V curve can be shifted to the left along the voltage axis by depolarizing prepulses (Armstrong and Bezanilla, 1977). This evidence implied that "activation" and "inactivation" are not independent parallel processes, as had been previously assumed, and supported the development of sequential kinetic models for the sodium channel. Slow inactivation, resulting from changes in holding potential, also affects the midpoint of the Q-V distribution. Bezanilla et al. (1982) showed that a change of holding potential from −70 to 0 mV moves the Q-V curve ~50 mV in a hyperpolarizing direction in squid axons. They interpreted their data as indicating that both the slow and fast inactivation gates must interact with the gating particles in such a way as to bias the reactivity of these gating particles to applied transmembrane potential. Alternatively, the Q-V curve could be shifted to the left by bias potentials resulting from charge rearrangements (or dipole movements) which are not directly related to channel gating. In this paper we shall demonstrate that the hyperpolarizing shift of the Q-V curve results from charge immobilization, although we leave open the question as to the whether "immobilization" (of I_g and "inactivation" (of I_{Na}) are equivalent processes.

Second, the Q-V curve is not necessarily a simple,

0006-3495/89/01/01/19 $2.00

symmetrical, sigmoid distribution. In contrast to the data obtained by Meves (1974) and by Keynes and Rojas (1974, 1976), Bezanilla and Armstrong (1975) showed that the Q-V curve obtained from a -70 mV holding potential shows two regions of differing slope: a low slope region negative to ~ -60 mV, leading to a high slope region visible at more depolarized test potentials. Bezanilla et al. (1982) suggested that such complex Q-V curves result from the differential weighting of gating particle subpopulations, biased to differing extents by coulombic interation with the fast and/or slow inactivation gates. In their model the charged inactivation gates were presumed to move parallel to the membrane surface such that they would not, themselves, generate any significant components of gating current.

Keynes (1986) has confirmed that, from -70 mV holding potential, the Q-V curve in squid axons shows two regions of differing slope. However he interpreted his data as suggesting that gating currents are produced by two independent conformational changes occurring in different parts of the sodium channel molecule. The low slope region of the Q-V curve could reflect a lower valence ($0.9e$) transition which is not affected by inactivation. The high slope region could reflect a second, inactivation-sensitive, conformation change with higher effective valence ($1.9e$). He did not discuss how this two gating particle model might be compatible with the simple sigmoid Q-V curve seen from a holding potential of -100 mV (Keynes and Rojas, 1976) in these same axons. Finally, Almers (1978) has questioned whether the low slope region of the Q-V curve has any direct relationship to sodium channel gating.

The primary aim of the present study has been to clarify the relationship between holding potential and the form of the Q-V curve. We shall demonstrate that the section of the Q-V curve which is obtained using depolarizing steps from holding potential always shows a high slope ($1.9e$). However, where a significant portion of the Q-V curve must be obtained using hyperpolarizing steps from holding potential, this region negative to the holding potential shows a lower slope of $\sim 0.75e$. Hence the fraction of total gating charge associated with the low slope component increases as holding potential is depolarized.

These results have been presented in preliminary form (see Starkus and Rayner [1988] and Rayner and Starkus [1988]).

METHODS

Preparation and data recording

Medial giant axons from the crayfish, *Procambarus clarkii,* with diameters between 200 and 300 μm, were internally perfused and voltage-clamped using methods previously described (Shrager, 1974; Starkus and Shrager, 1978; Starkus et al., 1984). Series resistance was compensated at 10 Ωcm^2 and corrections were made for an electrode junction potential of 8–10 mV. Temperature was measured with a thermilinear thermistor (Yellow Springs Instrument Co., Yellow Springs, OH) and was controlled to 6.0 ± 0.1°C by Peltier devices (Cambion Corp., Cambridge, MA). Electrode potential drift did not exceed 3–5 mV over 4–5 h of data recording. Experiments were carried out under computer control using a programmable pulse generator with 12 bit resolution, accurate to within ±0.1 mV (Adtech Inc., Honolulu, HI). Data traces were also digitized with 12 bit resolution using a Nicolet digital oscilloscope (model 1090A; Nicolet Instrument Corp., Madison, WI) and signal averaged on a Nicolet 1170. Sample intervals of 0.5, 1, or 2 μs/pt were used in this study. The signal averaged records (4090 data points) were then transferred and archived onto a hard disk unit (Century Data Systems, Los Angeles, CA) via a Dual 83/80 supermicrocomputer (Dual Inc., Berkeley, CA) running the UNIX system V operating system in a multiuser and multitasking mode. To compensate for the lack of real time processing ability on the UNIX system, a master program written in C language controlled external D/A and A/D devices during data acquisition. This master program also controlled data storage and retrieval, and provided data analysis procedures (including scaling, linear offsets, numerical integration, nonlinear least-squares fitting, and operator-controlled digital filtering).

Subtraction of linear capacity and leakage currents

The linear components of capacity and leakage currents were subtracted directly on the Nicolet 1170 signal averager, using a +P/n or −P/n procedure (Armstrong and Bezanilla, 1974; Bezanilla and Armstrong, 1977) modified to avoid artifacts associated with a slow component of capacity current (see Fig. 1 in Heggeness and Starkus, 1986). Since the time constant of this component is in the order of tens of milliseconds, all control pulses were preceded by a long conditioning period at the subtraction holding potential (SHP). The conditioning period was adjusted to be of sufficient duration (usually 50–100 ms) to permit complete relaxation of the slow capacity current. As shown in Fig. 1, cumulative artifacts can develop when shorter conditioning periods are used. Such artifacts distort the flat baselines required for accurate gating current integrations. Note the sloping baselines of traces *a* and *b* following conditioning periods of 5 and 20 ms, respectively, as compared with the flat baseline in Fig. 1 trace *c* after a 50-ms conditioning period. All control pulses in any P/n sequence must be separated by this same conditioning period. It is therefore our practice to return to holding potential between each pulse in a P/n sequence, to avoid prolonged holding at SHP.

It is equally important that P/n control pulses should be imposed within a voltage range where no significant gating charge movement is likely to occur. Bezanilla et al. (1982) have pointed out that gating charge movement might be expected in the standard negative range (-140 to -200 mV) after long-term inactivation induced by depolarized holding potentials. These authors therefore used a positive SHP as the base for their P/n control pulses in long-term inactivated axons. We demonstrate, see Fig. 2, *A* and *B*, that positive and negative SHP protocols give very similar results from a negative holding potential (-120 mV). However, in Fig. 2 *C* using data from a different axon, we show that any consistent differences between +SHP and −SHP control protocols remain small even after long-term inactivation at depolarized holding potentials. After conditioning periods as long as those used here, only negligible charge moves within the duration of typical P/n pulses from a negative SHP. Nevertheless, we have used the +SHP method

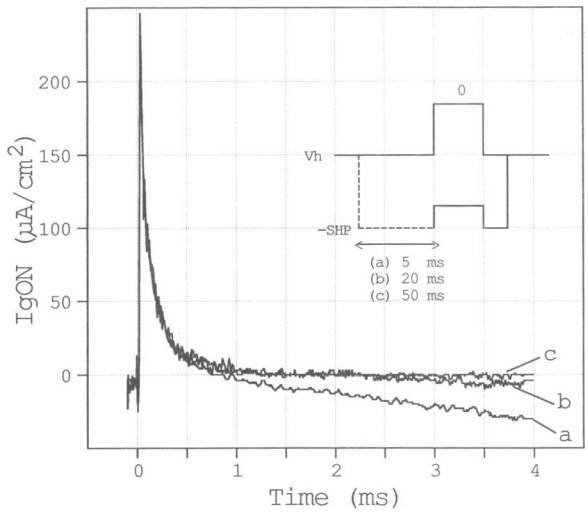

FIGURE 1 Distortion of gating currents by slow capacity transients. The step from holding potential to SHP occurs only in the P/n control pulse and is not matched within the test pulse pattern (see insert). Any remaining slow linear capacity current generated by this unmatched step appears, summed with the nonlinear gating current component, in capacity-subtracted traces. Such distortion is reduced when the duration of the conditioning period at SHP, before the P/n control step, is increased. Conditioning periods used here were: 5 ms, trace *a*; 20 ms, trace *b*; 50 ms, trace *c*. Axon 870514, step to 0 mV from holding potential of −120 mV, SHP −180 mV, P/4 protocol.

throughout the remainder of the study, to avoid any possibility of control pulse contamination by gating charge movement.

Nonlinear leak subtraction

Each gating current record was zeroed to a baseline by fitting a straight line through at least the last 1–2 ms of the data trace. A small offset is then apparent between the beginning region of each data trace (before the start of the voltage step) and the zero current line. For −SHP data (see Fig. 2 *A*), this initial offset represents a small nonlinear component of outward leakage current which becomes increasingly apparent in test pulses to more positive potentials. When +SHP protocols are used (see Fig. 2 *B* and also Fig. 2 of Bezanilla et al., 1982), this offset is larger and reversed in direction. Since the P/n control pulses now occur at potentials more positive than the typical test pulse, the nonlinear leak becomes greater in the summed controls than on the test pulse record. Hence the apparently reversed direction of the nonlinear leakage current in capacity-subtracted records from +SHP protocols.

Solutions

The external solution used throughout this study contained: tetramethylammonium (TMA), 210; Cl, 234; Mg, 2.6; Ca, 13.5; Hepes, 2 mM/liter. This solution was corrected to 430 mOsm/liter by addition of TMA chloride and adjusted to pH 7.55. Tetrodotoxin (TTX), obtained from Calbiochem-Behring Corp. (La Jolla, CA), was included at 200 nM/liter immediately before the experiment. The internal solution contained: TMA, 230; F, 60; glutamate, 170 mM/liter corrected to 430 mOsm/liter by addition of TMA glutamate and adjusted to pH 7.35. For the single experiment referred to here in which sodium ionic current was measured, the internal solution contained 50 mEq/liter Na with comparable reduction in TMA.

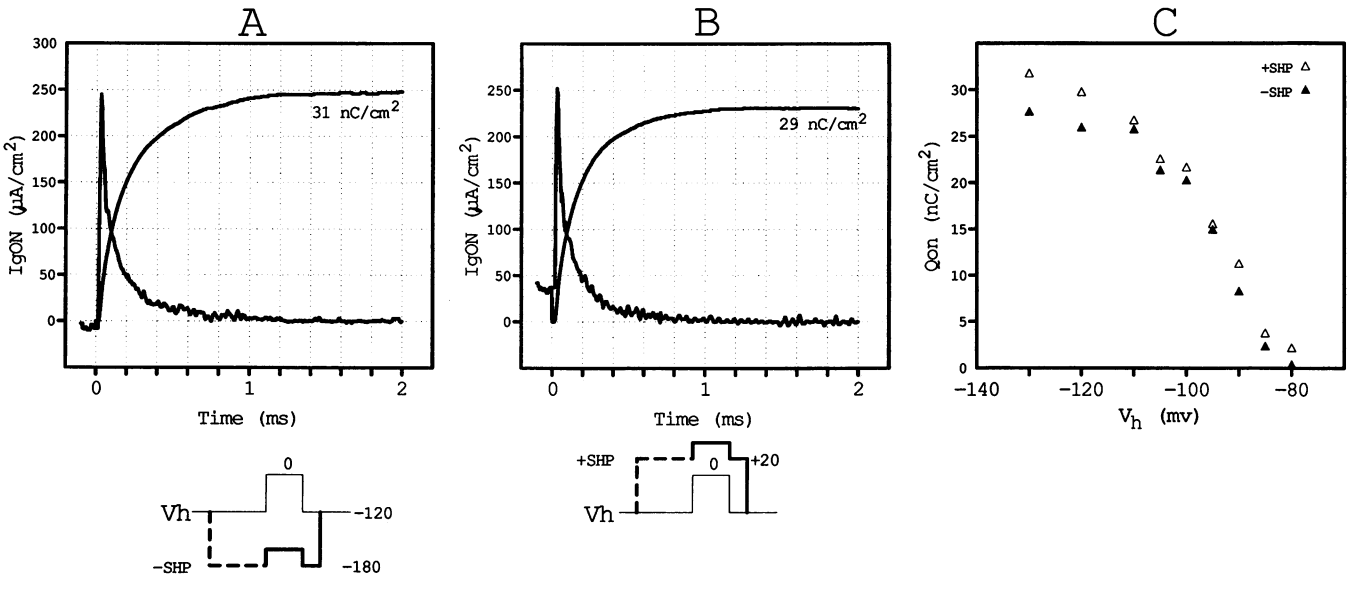

FIGURE 2 Negative and positive SHP protocols yield comparable gating current records. (*A*) Gating current by the negative SHP method for a step to 0 mV from −120 mV holding potential, SHP −180 mV, +P/4. (*B*) Gating current by the positive SHP method for the same voltage step as in *A*, SHP +20 mV, +P/4. (*C*) Comparison of charge movement from a different axon assessed using positive and negative SHP control pulses at holding potentials from −130 mV to −80 mV. *Open triangles*, SHP +20 mV, +P/4; *solid triangles*, SHP −180 mV, +P/4. (*A* and *B*) Axon 870514; (*C*) axon 870508.

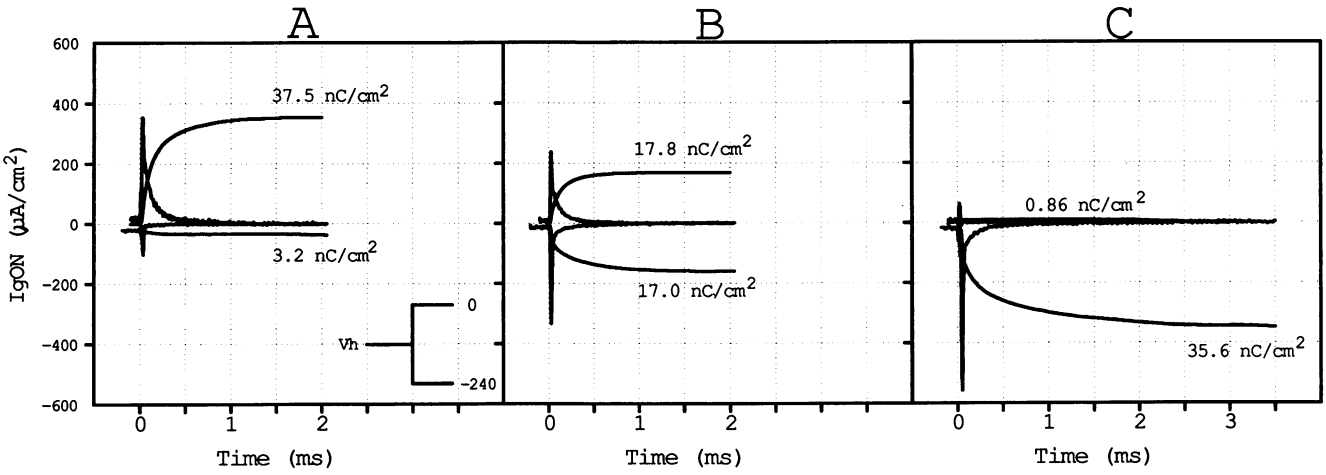

FIGURE 3 I_g recorded at −240 mV increases while I_g recorded at 0 mV decreases proportionately, as holding potential is shifted from −140 mV in *A*, to −100 mV in *B*, and to −70 mV in *C*. Axon 870604.

RESULTS

Changes in holding potential reveal a simple sigmoid, equilibrium gating charge distribution

In any Markovian system, each holding potential must be characterized by a unique voltage-dependent equilibrium between available conformational states. Thus where pulses to a constant test potential are used to evaluate the effect of holding potential (V_h) on test pulse gating charge (Q), the resulting Q-V_h relationship should reflect a true equilibrium distribution of the gating particles. Such an equilibrium distribution should be unaffected by whether a positive or negative test potential is chosen (provided that these test potentials are outside the voltage range in which detectable gating charge re-equilibration occurs). This hypothesis is examined in the data of Figs. 3 and 4.

Fig. 3 shows that, as holding potential is progressively shifted from −140 to −70 mV, gating current recorded in depolarizing steps (to 0 mV) progressively decreases, while charge moving in hyperpolarizing steps (to −240 mV) increases proportionately. In view of the necessary errors involved in the integration of small gating currents, it is hardly surprising that Q_{max}, the sum of the charge movements in depolarizing and hyperpolarizing steps, shows some variability at different holding potentials. In Fig. 3 we find that Q_{max} is 40.7, 34.8, and 36.5 nC/cm² at −140, −100, and −70 mV, respectively. However, we have noted that our estimates of total charge are consistently smaller from depolarized holding potentials (−60 or −70 mV) than from more negative holding potentials (such as −120 or −140 mV). As shown in Fig. 3 *C*, the rate of charge return becomes very slow when depolarized holding potentials are used and it is difficult to ensure that full charge recovery has been obtained. Thus the apparent Q_{max} observed from a holding potential of −70 mV was only 81% (±13% SD) of the Q_{max} seen in depolarizing steps from −140 mV, for the eight axons in

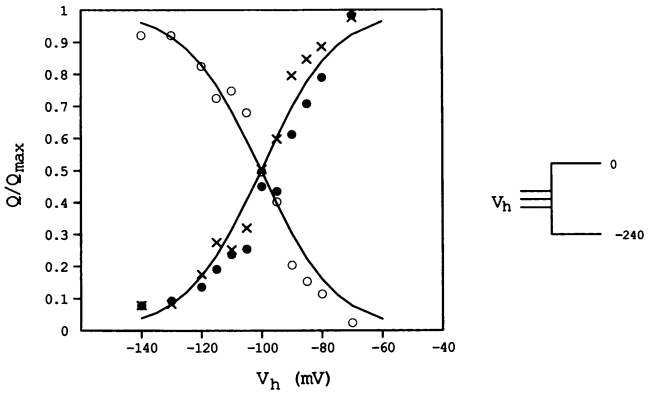

FIGURE 4 Change of holding potential (V_h) exposes a symmetrical equilibrium gating charge distribution. Gating currents were measured for each holding potential at both positive (0 mV) and very negative (−240 mV) test potentials, see pulse insert. *Open circles*, charge movements seen at 0 mV test potential were normalized to a Q_{max} of 39.5 nC/cm². *Crosses*, charge movements seen at −240 mV test potential were normalized against a Q_{max} of 34.9 nC/cm². *Solid circles*, charge movements recorded at 0 mV test potential, replotted as $(Q_{max} - Q_{on})/Q_{max}$. All data from axon 870604. The smooth curve with positive slope was drawn according to a standard Boltzmann equation: $Q/Q_{max} = 1/\{1 + \exp[-z(V - V_0)/kT]\}$ with an effective valence, z of 1.9e, where the midpoint, V_0, is at −100 mV and kT = 24.1 meV. The curve of negative slope was calculated as $(Q_{max} - Q)/Q_{max}$ for the same assumed parameters.

which both measurements were made. We have attempted to increase the accuracy of the Q_{max} seen in hyperpolarizing steps by using even more negative test potentials. This should increase the rate of return of gating charge, which would facilitate obtaining full charge within our gating current integrations. This has not been successful since membrane breakdown becomes an increasingly consistent problem below −240 mV in crayfish axons. Thus for the preliminary comparison shown in Fig. 4, gating currents seen in depolarizing steps to 0 mV test potential (*open circles*) were normalized against the Q_{max} recorded from −140 mV holding potential (39.5 nC/cm^2) in this axon. However, gating currents seen at −240 mV (*crosses*) were normalized against the Q_{max} measured from −70 mV holding potential (here 34.9 nC/cm^2). At least 2 min were allowed for equilibration after each change in holding potential and holding potentials were changed in a randomized order.

In Fig. 4, which gives typical data from a series of four similar experiments, both the curve showing gating charge moving in hyperpolarizing steps to −240 mV (*crosses*) and the equivalent curve for depolarizing steps to 0 mV (*open circles*) are well fitted by the same simple Boltzmann distribution. Furthermore when the curve obtained in depolarizing steps is inverted, by replotting the same data in the form $(Q_{max}\text{-}Q)/Q_{max}$, the resulting data points (*solid circles*) closely approximate the curve fitted to the data from hyperpolarizing voltage steps (*crosses*). These results seem fully consistent with the symmetry expected for a true equilibrium charge distribution. Thus the equilibrium distribution of gating charge (Q) as a function of holding potential (V_h) can be obtained with equal validity either: (*a*) from measurements of I_g at very negative test potentials (plotted directly as Q/Q_{max}), or (*b*) from measurements of I_g at positive test potentials plotted as $(Q_{max}\text{-}Q)/Q_{max}$. Throughout the remainder of this work $Q\text{-}V_h$ curves have been obtained by the second of these methods because of the increased accuracy of Q_{max} determinations from depolarizing pulse protocols.

We then initiated a series of experiments to obtain more accurate characterization of the $Q\text{-}V_h$ relationship. Holding potentials were changed in a randomized order, again allowing a 2-min equilibration period at each holding potential. Gating charge was measured at 0 mV test potential. At the start of each experiment we compared gating currents recorded at 0 and +20 mV to ensure that this test potential was sufficiently positive to produce full charge saturation. Rundown effects were avoided by inserting control pulses (from −120 mV holding potential to 0 mV test potential) after either each new holding potential or every second such measurment, depending on the stability of the axon studied. We were also careful to adjust the pulse repetition rates so as to avoid accumulation (or depletion) of slow inactivation during experimental pulse sequences at the different holding potentials. Q_{max} was assessed as the sum of charge moving in depolarizing steps (to +20 mV) and hyperpolarizing steps (to −200 mV) from −140 mV holding potential. From the ten experiments in this series which met our stability critera, we found the midpoint (Vo) of the $Q\text{-}V_h$ distribution to be at −102 mV ± 3 (SD) while Q_{max} was 37.2 nC/cm^2 ± 5.4 (SD). The ±15% variation in Q_{max} was removed by normalizing our data as $(Q_{max}\text{-}Q)/Q_{max}$, to facilitate comparison between axons. The normalized points were then transferred to linearized Boltzmann plots following the method introduced by Keynes and Rojas (1974, 1976). Linear regression was used to obtain a measure of the effective valence for each experiment. The correlation coefficients were 0.96 ± 0.03 (SD) for this data set, while the slopes of the regressions indicated a mean effective valence of 1.90e ± 0.23 (SD). A typical $Q\text{-}V_h$ curve from this sequence of experiments is shown in Fig. 6 (*solid circles*).

Q-V curves obtained using only depolarizing test pulses (from negative saturated holding potentials) are simple sigmoids which parallel the Q-V_h equilibrium charge distribution

Fig. 5 shows selected records from a family of gating currents obtained at different test potentials. Holding potential was −140 mV, which has been seen (Fig. 4) to be close to the negative end of the $Q\text{-}V_h$ distribution. Fig. 5 also demonstrates that a 2-ms integration period appears sufficient to measure the charge moving in each of these gating currents. Fig. 6 shows the $Q\text{-}V$ curve (*open squares*) obtained by plotting the areas under the gating currents of this data set against test potential. For reasons which will become apparent later in this paper, we shall refer to $Q\text{-}V$ curves obtained using only depolarizing pulses from holding potential as $Q\text{-}V_{dep}$ curves. Charge movement remains small between V_h and −80 mV but increases steeply thereafter to saturate at ~0 mV. A steady state $Q\text{-}V_h$ curve (*solid circles*) from a different axon has been included in this figure for comparative purposes. The similar voltage reactivity of the $Q\text{-}V_{dep}$ and $Q\text{-}V_h$ distributions is demonstrated in Fig. 6, by the similar slopes of the data points. The curves drawn through both the $Q\text{-}V_{dep}$ and the $Q\text{-}V_h$ data were calculated assuming a Boltzmann distribution with valence of 1.9e. From a series of six experiments at holding potentials of −140 or −120 mV, the mean slope of the $Q\text{-}V_{dep}$ distribution was 1.79e ± 0.15 (SD) and the midpoint of this distribution was at −53 mV ± 4 (SD).

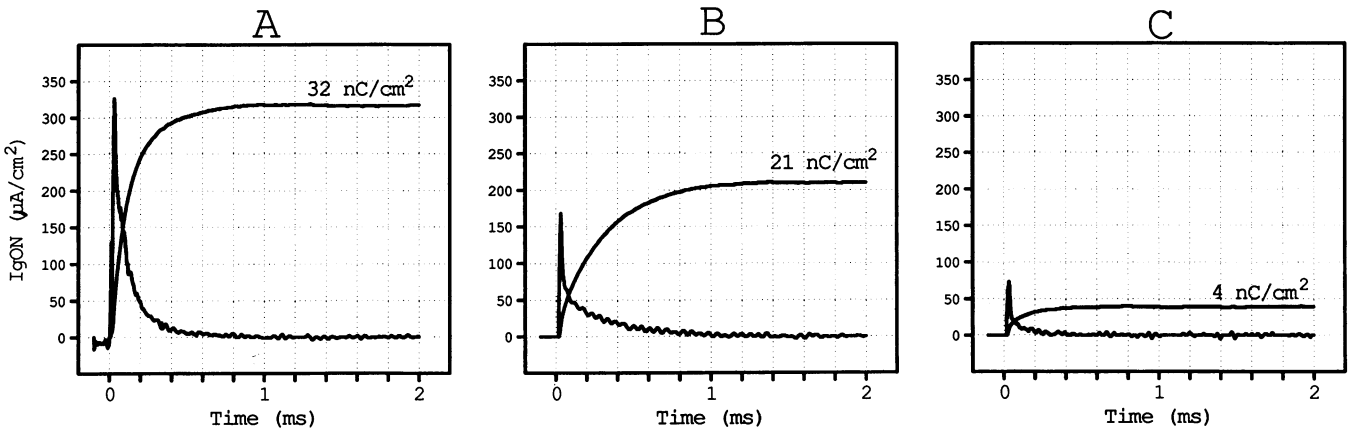

FIGURE 5 ON gating currents and their integrations recorded at test potentials of 0 mV (*A*), −40 mV (*B*), and −80 mV (*C*). Holding potential −140 mV, axon 870507.

Two main conclusions can be derived from the data presented in Figs. 5 and 6:

(*a*) *Substantial gating charge movements can occur without producing experimentally detectable gating currents.* As shown in Fig. 5 *C*, for example, the gating current in a step from −140 to −80 mV appears complete within 2 ms, during which time some 12–15% of total charge crosses the membrane. This data point is also shown at −80 mV on the Q-V_{dep} curve in Fig. 6 (*open squares*). By contrast, the Q-V_h curve (Fig. 6, *solid circles*) indicates that more than 90% of total charge has crossed the membrane at −80 mV after a 2-min equilibration period. Thus, at −80 mV, as much as 75% of total charge apparently crosses the membrane at rates so slow that this charge movement was not detected in our Fig. 5 *C* gating current measurement. Is this conclusion reasonable, or should some other explanation be sought for the 60 mV shift to the left (see Fig. 6) of the Q-V_h curve relative to the Q-V_{dep} distribution?

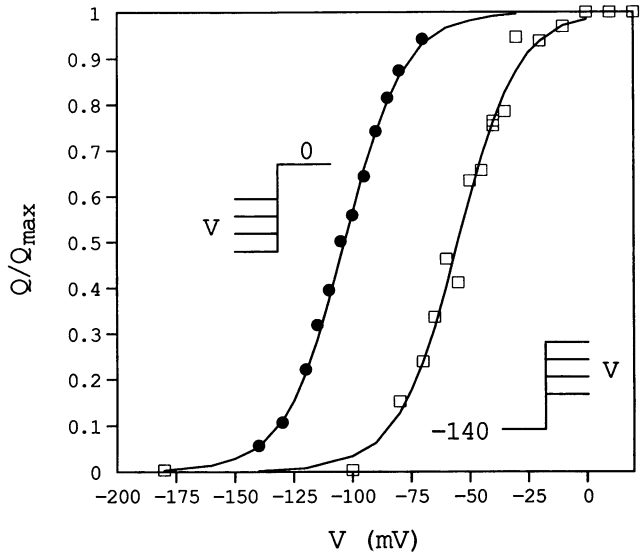

FIGURE 6 The Q-V curve (*open squares*), obtained by integration of I_g records at differing test potentials from −140 mV holding potential, is displaced about 60 mV in the depolarizing direction from the equilibrium gating charge distribution (*solid circles*). Q-V data points from axon 870507. Q-V_h data from axon 870609. Q_{max} was 32.4 nC/cm² for axon 870507 and 43.4 nC/cm² for axon 870609. Smooth curves were drawn as in Fig. 4, with $z = 1.9e$ in both cases. V_0 was −55 mV for the Q-V curve and −103 mV for the Q-V_h curve.

In experimental records such as those shown in Figs. 1, 2, 3, and 5, the practical limit of gating current resolution depends on the ability to distinguish real from artifactual transients when determining the point at which I_g disappears into the baseline of nonlinear leak (see Methods). It is routine for us to ignore any slope less than ~2 μA/cm² per ms. However, where total gating charge is ~40 nC/cm², a gating current of 2 μA/cm² would permit as much as 50% of total charge to cross the membrane in 10 ms. A maintained gating current of 0.2 μA/cm², which is well below the limits of our normal resolution, would move 50% of total charge in 100 ms (a short time by comparison with the seconds or minutes required for full charge equilibration). It is thus entirely possible that substantial slow charge movements might occur which would not be readily resolvable within a standard Q-V protocol.

(*b*) *No significant additional valence is involved in the equilibration process by which the Q-V_h distribution is shifted to the left of the Q-V_{dep} curve.* The similar slopes of the Q-V_{dep} and Q-V_h curves in Fig. 6 indicate that the

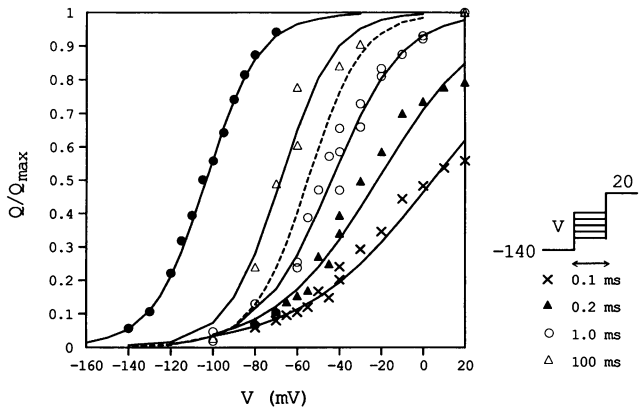

FIGURE 7 The isochronal Q-V_{dep} curve for 100-ms prepulses (*open triangles*) shows similiar reactivity to the Q-V curve shown in Fig. 6 (*dashed line*) and the equilibrium charge distribution from that same figure (*solid circles*.) For prepulse durations shorter than 2 ms apparent valence increases as a function of prepulse duration. Prepulse durations were 100 μs (*crosses*), 200 μs (*solid triangles*), and 1 ms (*open circles*). Isochronal curves for 100 and 1 ms represent pooled data from axons 870623, 870624, and 870626; Q_{max} values were 28.8, 36.8, and 38.8 nC/cm² in these axons. Isochronal curves at 100 and 200 μs were from axon 870507, where Q_{max} was 32.4 nC/cm². Smooth curves were drawn according to the parameters of fit shown below.

	Parameters of fit					
	Q-V_h	100 ms	Q-V	1 ms	0.1 ms	0.2 ms
z	1.9e	1.9e	1.9e	1.45e	0.77e	0.99e
V_0	−103 mV	−68 mV	−55 mV	−43 mV	0 mV	−30 mV

primary voltage reactivity of the gating particles must already have been expressed by the end of the integration period (~2 ms) used to characterize the Q-V_{dep} curve in this experiment. It follows that the additional slow charge movement, involved in the approach to the equilibrium Q-V_h distribution, results from apparently voltage insensitive processes.

Fortunately an experimental method is available which provides the additional precision required to confirm both conclusions *a* and *b* above. We used a negative holding potential (−140 mV) to maximize charge movement in the test pulse. We then evaluated the suppression of test pulse gating charge (Q_{test}), at constant test potential (+20 mV), after prepulses of differing potential and/or duration (see Fig. 7, pulse pattern insert). In these experiments Q_{max} was determined as the sum of the maximum hyperpolarizing and depolarizing charge movements from −140 mV holding potential, while the standard ordinate, Q/Q_{max}, was determined experimentally as $(Q_{max} - Q_{test})/Q_{max}$. For prepulses of constant duration to varying potentials, this method generates "isochronal" Q-V_{dep} curves (see Fig. 7). Alternatively, using prepulses of differing durations, one can track the rate of charge equilibration at selected prepulse potentials (see Fig. 8).

Fig. 7 compares isochronal Q-V_{dep} curves to the Q-V_h curve (*solid circles*) and standard Q-V_{dep} curve (*dashed line*) from Fig. 6. The isochronal prepulse protocol was utilized firstly to evaluate charge movement during 100-ms steps (*open triangles*). The resulting 100-ms isochronal curve (with slope of 1.93e) parallels both the steady-state Q-V_h distribution (*solid circles*) and the standard Q-V_{dep} curve (*dashed line*). Thus at all potentials between about −90 and −50 mV the fraction of gating charge moving between 2 and 100 ms is independent of potential, as would be expected if the rates governing slow charge movements were essentially voltage independent.

The isochronal approach was next used to examine the movement of gating charge at times earlier than 2 ms, where voltage-sensitive charge movement would be expected. Fig. 7 shows the isochronal Q-V curves obtained for 100 μs, 200 μs, and 1 ms prepulse durations. The slopes of these curves were 0.77e, 0.99e, and 1.43e, respectively, obtained from linearized Boltzmann plots (as in Fig. 12). During voltage-sensitive gating charge movement it is clear that the apparent valence increases with increasing prepulse duration. However these data also demonstrate that Q-V curves will give a low valence estimate, without departure from an apparent fit to the

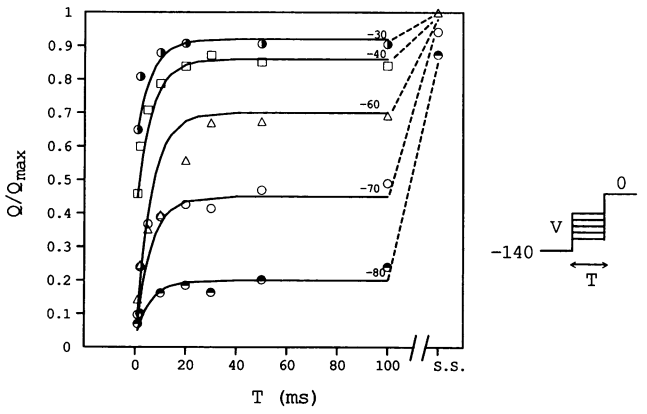

FIGURE 8 Charge movements associated with equilibration during prolonged depolarizing pulses may be characterized using a prepulse method (see pulse pattern insert). Prepulse data is from axon 870624, with a Q_{max} of 36.8 nC/cm². Prepulse potentials used were −80, −70, −60, −40, and −30 mV. Smooth curves were fitted to the data points between 0.5 and 40 ms, assuming a single time constant of 6 ms at all prepulse potentials. Steady-state values (S.S.) are included from axon 870609 (see Fig. 6) for comparison with the apparent plateaus shown in each curve at times greater than ~30 ms.

Boltzmann distribution, wherever technical limitations prevent collection of the full voltage-sensitive I_g component. This problem is minimized in crayfish axons both by their increased charge density (2,300 e/μm^2 seen here, as compared with 1,500 to 1,900 e/μm^2 for squid axons, see Hille, 1984) and by their two- to threefold more rapid gating current kinetics (see Starkus et al., 1981). Finally, these results place considerable constraints on possible models for the channel mechanism, since the midpoint of the gating charge distribution changes so markedly as a function of prepulse duration: from ~0 mV for a 100-μs prepulse, to −30 mV for a 200-μs prepulse, to −43 mV at 1 ms, −55 mV at 2 ms, −75 mV at 100 ms, and to −100 mV under equilibrium conditions.

Fig. 8 shows additional data from the same series of prepulse experiments. Data points were obtained at selected prepulse potentials across a larger range of prepulse durations, to demonstrate the time course of charge equilibration at each of these potentials. In each curve the first point plotted is for a 1-ms prepulse, so that voltage-sensitive charge movements are largely excluded from this plot. At all potentials an initial rapid phase of voltage-insensitive charge movement is evident. In each curve this phase has been fitted with the same 6-ms time constant; we have called this the "fast equilibration component." Thereafter steady-state levels are approached by rates so slow that they cannot be evaluated from the data shown here. However, the relative importance of the fast and slow equilibration processes changes with depolarization, although the kinetics of these processes appear voltage insensitive. Thus at −80 mV, the fast equilibration component moves 10% whereas slow equilibration processes move 65%. The fractions of total charge moving at the fast and slow equilibration rates are nearly reversed at −40 mV, where the fast equilibration component accounts for ~40% whereas slow charge equilibration moves only 15% of total charge. Although not shown in Fig. 8, at potentials more positive than 0 mV essentially all charge movement occurs within the time period associated with voltage-sensitive charge movements (i.e., <2 ms).

At this point it seems appropriate to note, from the data of Fig. 8, that the limit of practical charge resolution would be a slope of ~5% of total charge moving in 100 ms. The resolution of this method is thus some two orders of magnitude greater than that available from direct gating current measurements at the less depolarized prepulse potentials. However the data obtained by the prepulse method fully confirm the conclusions reached from the more traditional approach, namely that large charge movements may occur at rates too slow to be detected in typical gating current measurements and, second, that these slow charge movements occur at voltage-insensitive rates.

Q-V curves obtained using hyperpolarizing test pulses (from depolarized holding potentials) show lower slopes than the Q-V_h curve

When the membrane is held at potentials close to the depolarized end of the Q-V_h curve, the voltage sensitivity of return charge movement can be investigated using hyperpolarizing voltage steps. In crayfish axons −70 mV is a reasonable holding potential for this purpose (although it is potentially confusing that in squid axons −70 mV seems to lie near the hyperpolarized end of the steady-state curve). We shall refer to Q-V curves obtained using only hyperpolarizing pulses as Q-V_{hyp} curves, so as to distinguish them from the Q-V_{dep} curves described in the previous section. Recovery of gating charge during hyperpolarizing prepulses was assessed from changes in test pulse gating current at 0 mV test potential (see Fig. 9, pulse pattern insert). Pulses from −140 mV holding potential to 0 mV were inserted to monitor Q_{max} throughout the data collection period.

Fig. 9 shows a representative set of isochronal Q-V_{hyp} curves collected using this prepulse protocol from a holding potential of −70 mV. The data points shown here were fitted by smooth curves assuming apparent valencies of 0.6e for 1-ms prepulses (*open circles*), 0.75e for 6-ms prepulses (*open squares*), and 1.0e for 100-ms prepulses (*open triangles*). The assumptions required for this curve fitting procedure are fully described in the Discussion and Appendix. It is apparent that the data points for different prepulse durations do not lie parallel to the Q-V_h distribution. These data were readily repeatable and the mean slope obtained from four 6-ms prepulse experiments from −70 mV holding potential was 0.73 ± 0.04 (SD). The results presented here for hyperpolarizing pulses from −70 mV holding potential are thus in sharp contrast to the data of Fig. 7 for depolarizing prepulses of similar duration. On the other hand the changes in slope of these Q-V_{hyp} curves appear entirely equivalent to the changes in slope seen for Q-V_{dep} curves with prepulses of durations <2 ms, where voltage sensitive charge movement is occurring. We conclude that recovery from depolarized holding potential is similarly a voltage-sensitive process. However in these hyperpolarizing voltage steps gating charge recovery remains voltage sensitive for at least 100 ms, if not until steady state is reached.

An equivalent result is demonstrated by a more direct method in Fig. 11 *A*, where changes in prepulse duration at selected prepulse potentials were used to examine the voltage sensitivity of charge re-equilibration rates (cf. Fig. 8). We concentrated on the rates of charge return at −180 and −200 mV since it was in this very negative range that we expected the greatest voltage sensitivity, if

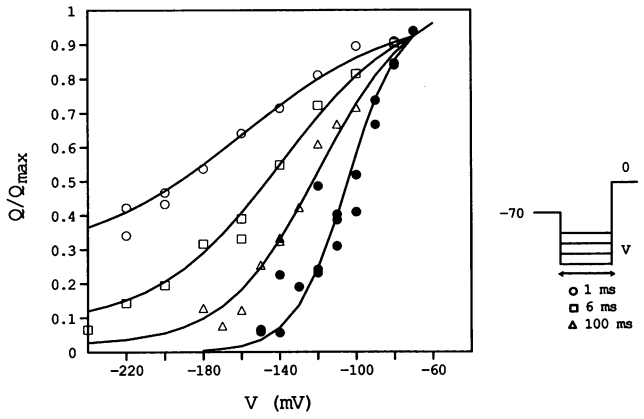

FIGURE 9 Isochronal Q-V curves from depolarized holding potentials do not run parallel to the equilibrium gating charge distribution. Apparent slope increases with increasing prepulse duration. Prepulse durations were 1 ms (*open circles*), 6 ms (*squares*), and 100 ms (*triangles*). *Solid circles* indicate steady-state data obtained by change of holding potential. The Q-V_h data and the 6- and 100-ms prepulse data was from axon 870702 with Q_{max} of 38.0 nC/cm^2. Data for 1-ms prepulses came from axon 871021 where Q_{max} = 46.2 nC/cm^2. The smooth curve through the Q-V_h data was drawn (see legend for Fig. 4) assuming z = 1.75e and V_0 = −104.5 mV. Curves were fitted to the isochronal data points as described in the Appendix, using the following parameters of fit (see Appendix for explanation of symbols used).

	Parameters of fit			
Prepulse durations	1 ms	6 ms	100 ms	Q-V_h
V_0	−160	−140	−120	−104.5 mV
z	0.6	0.75	1.0	1.75e
s_s	0.28	0.08	0.02	—
q_h	0.923	0.923	0.923	—

any, would occur. Complete recovery was achieved by 500 ms at −200 mV but took more than 1 s at −180 mV. The early recovery rates shown here also seem voltage dependent, with about a twofold difference in time constant between the −180 and −200 mV data. In contrast to the depolarization-induced charge equilibration rates studied in Fig. 8, both the fast and slow rates of return charge equilibration show clear voltage sensitivity. Thus voltage sensitivity charge movement, which is completed within 2 ms for depolarizing voltage steps, continues for more than 200 ms after hyperpolarizing voltage steps.

We conclude that some "asymmetry" must exist in the control mechanism of the crayfish sodium channel, such that the membrane shows different characteristics in response to depolarizing and hyperpolarizing pulses. We shall later demonstrate (see Discussion) that such asymmetry is not entirely unexpected since it seems a necessary property of models in which voltage-sensitive pre-open transitions are coupled to voltage-insensitive charge-immobilizing reactions. Nevertheless this observation further restricts the possible models which may be used to describe the steady-state properties of the sodium channel.

If this result can be generalized to other axons, the asymmetry we have observed poses interesting experimental problems which may not have been fully appreciated in previous studies. Any full Q-V curve, obtained from a nonsaturated holding potential, requires hyperpolarizing pulses to delineate the region negative to the holding potential and depolarizing pulses for the section positive to the holding potential. Our results would seem to predict that the region of the Q-V curve found using hyperpolarizing pulses will necessarily show a reduced slope, as in Fig. 9, characteristic of Q-V_{hyp} data. By contrast the "high slope" region of the Q-V curve, obtained using depolarizing pulses, might be expected to show the simpler characteristics of Q-V_{dep} curves. Our findings thus suggest an alternative hypothesis to explain the simple sigmoid Q-V curve reported in squid axons by Keynes and Rojas (1976) from a holding potential of −100 mV, as compared with the more complex curves reported by both Bezanilla and Armstrong (1975) and Keynes (1986) for these axons at −70 mV holding potential. This hypothesis is further evaluated in the following section.

Q-V curves change their shape with change of holding potential

Fig. 10 shows Q-V curves obtained from holding potentials of −140, −120, −100, and −80 mV. To facilitate comparison with previous published work, each curve was obtained using the standard experimental technique involving depolarizing and/or hyperpolarizing test pulses from holding potential (see Fig. 10, pulse pattern insert). Integration periods required were 2–4 ms for depolarizing pulses and 6–8 ms for hyperpolarizing test pulses. All data points were normalized with respect to Q_{max} values determined in depolarizing pulses from a negative saturated holding potential (here −140 mV) to positive test potentials (0 and +20 mV). Control pulses from −120 mV holding potential to 0 mV test potential were interspersed within the data set to control for possible run-down. All data shown here, except the −140 mV Q-V curve (*sold triangles*), came from a single, highly stable, axon.

From −140 mV, which is near the hyperpolarized end of the Q-V_h distribution, a simple sigmoid Q-V curve (*solid triangles*) was obtained. This curve appears similar in shape to that reported for squid axons from −100 mV holding potential by Keynes and Rojas (1976). Negligible

charge movement was found in hyperpolarizing pulses from so negative a holding potential. Thus the entire charge movement could be characterized from depolarizing voltage steps. The mean Q-V valence obtained from -140 mV holding potential in four experiments was $1.85e \pm 0.09$ (SD).

From a holding potential of -120 mV, the Q-V curve (*open triangles*) appears more complex. Significant charge now moves in hyperpolarizing test pulses, with the lower apparent voltage reactivity which would be expected from our Q-V_{hyp} data. On the other hand, the charge movement collected in depolarizing voltage steps shows the steeper slope characteristic of both the steady-state Q-V_h curve (*solid circles*) and the Q-V curve from -140 mV holding potential (*solid triangles*). Thus the -120 mV Q-V curve separates into low and high slope regions, appearing very similar to Q-V curves obtained in squid axons held at -70 mV (see Bezanilla and Armstrong, 1975; Armstrong, 1981; Keynes, 1986). It is interesting that the visible discontinuity of slope does not occur at the holding potential (-120 mV) but rather at ~ -100 to -80 mV where a steep increase in charge movement is also seen in the -140 mV curve. Similarly Armstrong (1981) has noted for squid axons held at -70 mV, that the apparent discontinuity of slope does not occur at the holding potential. The small section of the Q-V curve between holding potential and this apparent "threshold" for ON charge movement is not easily characterized by experimental data. However, the controlling effects of holding potential on the shape of the Q-V curve become increasingly apparent when more depolarized holding potentials (-100 and -80 mV) are used.

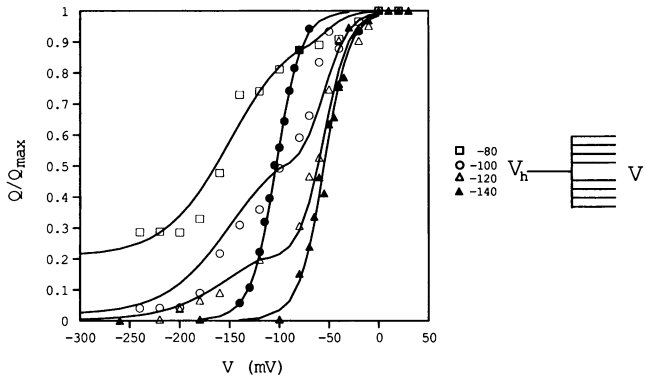

FIGURE 10 Q-V curves change in shape after change of holding potential. From -140 mV holding potential (*solid triangles*) a simple sigmoid Q-V curve parallels the equilibrium charge distribution (*solid circles*). Q-V curves obtained at the following nonsaturated holding potentials: -120 mV (*triangles*), -100 mV (*open circles*), and -80 mV (*squares*) show low and high slope regions (see text and pulse pattern inserts for further description of experimental protocols). Data from -140 mV holding potential was from axon 870507; data from holding potentials of -80 mV, -120 mV, and -100 mV, as well as the Q-V_h data, came from axon 870609. Smooth curves were drawn using the following parameters of fit (see Appendix).

At holding potentials of -100 and -80 mV, the Q-V curves also divide into regions of differing slope following a similar pattern with respect to holding potential to that seen at -120 mV. The apparent changes in slope seem entirely consistent with the characteristic asymmetry we have already noted in response to hyperpolarizing versus depolarizing voltage steps (presuming that the Q-V_{dep} component has the same slope and the same midpoint at all holding potentials). In three axons where we have evaluated the Q-V_{dep} component from a holding potential of -100 mV, the mean valence was found to be $1.70e \pm 0.22$ (SD) with a midpoint of -50 ± 5 mV. For comparison the mean valence of the Q-V_{hyp} component in these same axons was $1.03e \pm 0.30$ (SD) with a midpoint of -158 ± 9 mV.

In Fig. 10 we confirm that the high slope component is reduced when charge immobilization is increased by shifting to more depolarized holding potentials, as reported in Keynes (1986). However, the fraction of Q_{max} which moves with lower apparent valence also changes markedly with holding potential, being negligible when V_h is -140 mV, small (8.6 nC/cm^2) for the -120 mV Q-V curve, larger (21.3 nC/cm^2) at -100 mV holding potential, and further increasing to 37.9 nC/cm^2 at -80 mV holding potential, as compared to a Q_{max} of 43.4 nC/cm^2 for this same axon. These results provide additional data in support of our hypothesis that the high and low slope regions of the Q-V curve result from asymmetry in the responses of the sodium channel to depolarizing and hyperpolarizing pulse directions.

Parameters of fit (positive to V_h)					Parameters of fit (negative to V_h)			
Holding potential	-140	-120	-100	-80	Holding potential	-120	-100	-80
V_0	-55	-55	-55	-55	V_0	-150	-150	-150 mV
z	1.90	1.90	1.90	1.90	z	0.75	0.75	$0.75e$
s_s	0	0.19	0.48	0.86	s_s	0.00	0.02	0.21
q_h	0	0.20	0.49	0.87	q_h	0.20	0.49	0.87

During hyperpolarizing prepulses test pulse I_{gON} recovers more rapidly than I_{Na}, after long-term inactivation

Bezanilla et al. (1982) noted that I_{gON} recovers more rapidly than I_{Na} from the effects of depolarized holding potentials during prepulses to −130 or −170 mV in squid axons. Fig. 11 *B* demonstrates that I_{gON} and I_{Na} also recover at different rates in crayfish giant axons during strongly hyperpolarizing prepulses from −70 mV holding potential. About 30% recovery of I_{gON} must occur before any significant sodium current becomes visible. Thereafter recovery of I_{Na} occurs more rapidly than I_g until a similar fractional recovery is obtained for both I_{Na} and gating current. The final slow I_{Na} recovery may well be limited by the rate of recovery of gating charge.

There is no major shift in the voltage sensitivity of depolarization-induced charge movement after long-term inactivation

Fig. 9 shows 85–90% recovery of test pulse gating charge after 6-ms prepulses to −200 mV. Although recovery was assessed from the gating charge movement within a subsequent test depolarization to 0 mV, it has not yet been shown whether this gating charge moves with normal or "left-shifted" voltage sensitivity within the depolarizing test pulse. Interrupting the return to test potential with a brief pause at −140 mV should clarify the voltage range in which major charge movement occurs (see Fig. 11 *C*, pulse pattern insert). As shown in Fig. 11 *C*, only very minimal charge movement occurred in the first depolarizing step from −200 to −140 mV (*open squares*) at all prepulse durations from 0.5 to 500 ms. Clearly the major charge movement occurred in the second depolarizing step (*open circles*) between −140 and 0 mV. There is thus no evidence of any major change in the voltage sensitivity of the gating charges after long-term inactivation in these crayfish axons.

DISCUSSION

The principal results of this study can be summarized as follows:

(*a*) Successive changes of holding potential expose a symmetrical equilibrium gating charge distribution (the Q-V_h curve) with an apparent valence of 1.9*e* and a midpoint at ~−100 mV (see Fig. 4).

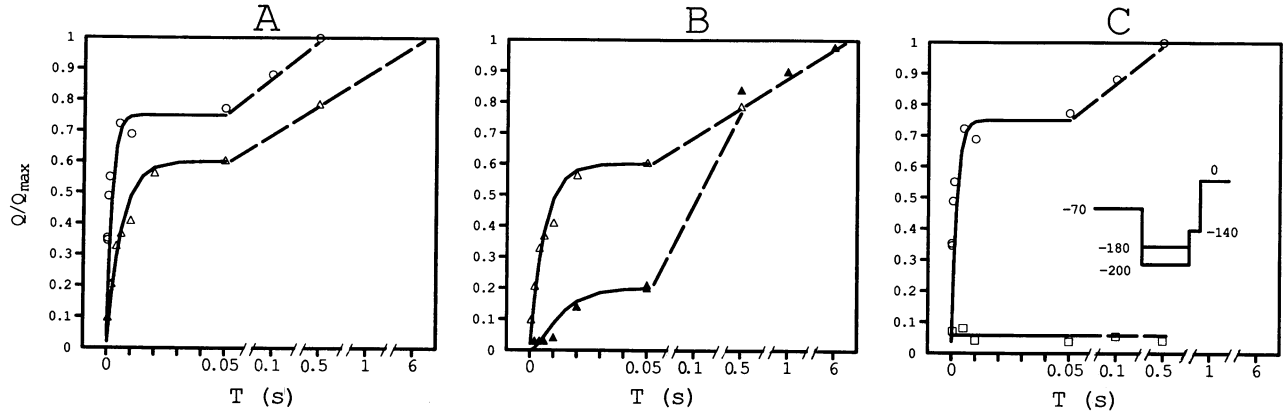

FIGURE 11 (*A*) Recovery of gating charge, following long-term inactivation at −70 mV holding potential, is incomplete in the millisecond time range even at very negative potentials. Charge recovery was assessed during prepulses from −70 mV to −200 (*circles*) or −180 mV (*open triangles*), and normalized against Q_{max} determined in a step from −140 mV holding potential to 0 mV in these same axons. Continuous curves were drawn presuming fast time constants of 2 ms at −200 mV and 6 ms at −180 mV. Data for −200 mV were from axon 870612 with a Q_{max} of 34.0 nC/cm²; −180 mV data was combined from axons 870422 and 870424 where the mean Q_{max} was 37.8 nC/cm². (*B*) I_{Na} recovers less completely than gating charge during the initial recovery phase after long-term inactivation. Recovery of I_{Na} (*solid triangles*) is compared with recovery of gating charge (*open triangles*) during prepulses to −180 mV from a holding potential of −70 mV. Continuous curves were drawn presuming a fast time constant of 6 ms for charge recovery; I_{Na} recovery was modeled as a two-step sequential process leading to recovery of the open state, with time constants of 6 and 8 ms, respectively. Data for charge recovery were combined from axons 870422 and 870424; I_{Na} recovery data were from axon 870422. (*C*) Long-term inactivation does not seem to alter the voltage range within which ON charge movement appears. After prepulses to −200 mV from −70 mV holding potential, a divided test pulse was used (see pulse pattern insert) to assess the voltage range in which ON charge movement occurred. Step one was from −200 mV to −140 mV; charge moving in this step (*squares*) was small at all prepulse durations. Step two was from −140 mV to 0 mV; charge moving in this step (*circles*) demonstrates time-dependent recovery. The interval between steps one and two was held constant at 500 μs; gating currents generated in step one had in all cases fallen to less than 1 μA/cm² by the end of this interval. All data were from axon 870612.

(*b*) Voltage-sensitive depolarization-induced gating charge movement is completed within ~2 ms, in these axons, yielding a Q-V_{dep} curve with parallel slope to the Q-V_h curve but with a midpoint at ~ −40 mV (see Figs. 6 and 7).

(*c*) In more prolonged depolarizations, this quasi steady-state Q-V_{dep} distribution returns towards the equilibrium Q-V_h curve by processes which appear to be almost voltage independent (see Figs. 7 and 8).

(*d*) By contrast, no equivalent quasi–steady state can be detected for hyperpolarization-induced gating charge movement and the slopes of Q-V_{hyp} curves are significantly less than would be expected from the apparent valence of the equilibrium charge distribution (see Fig. 9).

(*e*) Q-V curves from intermediate holding potentials (see Fig. 10) show a low slope region, negative to the holding potential, obtained from hyperpolarizing voltage steps and a relatively high slope region obtained from depolarizing voltage steps.

Interpretation of these results requires that we first recognize the clear quantitative differences between squid and crayfish preparations. The resting potentials of intact crayfish axons range between −95 and −100 mV, which is some 30 mV more negative than in squid. Additionally, TTX at the concentration used here induces a further 10 mV shift in the midpoint of the steady-state gating charge distribution from −90 to −100 mV (Heggeness and Starkus, 1986). Thus the holding potentials used in our work are ~40 mV more negative than would be required to collect equivalent data from squid axons. However the midpoint of the Q-V_{dep} distribution shows only a 20 mV shift, being ~ −40 mV in crayfish as compared with −20 mV in squid. It follows that the shift to the left of the Q-V_h versus Q-V_{dep} distribution, which is as much as 60 mV for crayfish (see Fig. 6), may be only about half that amount in squid axons. The Q-V_h distribution has not yet been characterized in squid axons. However the data in Fig. 5 of Bezanilla et al. (1982) is sufficient to provide an estimate of the Q-V_h midpoint voltage, presuming that the Q-V_h curve in squid is also a simple Boltzmann distribution parallel to the Q-V_{dep} curve. At −70 mV holding potential Q/Q_{max} was ~0.2 in their figure; assuming z = 1.6e for their data and solving Eq. 1 (see Appendix) for the midpoint gives −50 mV, again suggesting that the Q-V_{dep} and Q-V_h curves are separated by only ~30 mV in squid axons.

Despite these quantitative differences, our work remains consistent with much squid axon data. We have confirmed the shifts of the Q-V curve seen after depolarizing prepulses by Armstrong and Bezanilla (1977), as well as following depolarized holding potentials by Benzanilla et al. (1982). Additionally we confirm that the Q-V curve has a simple sigmoid form when investigated using depolarizing pulses from very negative holding potentials (see Keynes and Rojas, 1976). However, two regions of different slope become apparent when less negative holding potentials are used (see Bezanilla and Armstrong, 1975; Armstrong, 1981; Keynes, 1986). The effective valence of the gating particles was first measured as 1.3e by Keynes and Rojas (1974, 1976). Later, the high slope region was fitted with 1.6e by Bezanilla et al. (1982), 1.9e by Keynes (1986), and 1.9e in the present study. Our work has provided an explanation of the higher valence estimates of more recent studies. As shown in Fig. 7, a lower valence must necessarily be found if technical limitations prevent integration of the full voltage-sensitive component of charge movement. Thus when we reduced the charge collection period from 2 to 1 ms, the slope of the Q-V curve fell from 1.9e to 1.4e. We also note, as pointed out by Keynes (1986), that the fraction of total gating charge carried in the high slope component of the Q-V curve becomes progressively reduced when more depolarized holding potentials are used, as if this component of the Q-V curve is sensitive to inactivation and/or charge immobilization.

On the other hand our results have provided new constraints against which such conclusions can be evaluated. We show (see Fig. 10) that as holding potential is made more negative, the low slope component of the Q-V curve becomes progressively smaller, without any change in Q_{max}, until it finally disappears. The charges which move in hyperpolarizing pulses to generate the low slope component cannot reflect a separate, discrete, population of "low valence particles" if they can be converted into "high valence particles" by shift of holding potential. The suggestion of Almers (1978), that the low slope region might reflect nonspecific charge movements not involved in sodium channel gating, is similar to the model presented by Keynes (1986) in that both require discrete particle populations with differing valences. Both hypotheses would seem ruled out by our observations here, although we are left with a curious paradox: how can particles change from low to high effective valence without detectable change in Q_{max}? Clearly either the measurement of Q_{max} or the measurement of effective particle valence must be incorrect in these data (if we are to avoid the conclusion that a smaller number of high valence particles disaggregates into a larger number of low valence particles as holding potential is depolarized).

Q_{max} in the data of Fig. 10 was particularly carefully assessed. The Q-V curves for V_h = −80, −120, and −100 mV were obtained from the same axon, in that order. Frequent control pulses demonstrated the absence of any significant rundown during collection of this data set, and the same Q_{max} value of 43.4 nC/cm^2 was used to normal-

ize each curve. It is clear that the fraction of charge moving in the low slope portion of the Q-V curve changes with change of holding potential.

The differences between gating charge movements observed in response to depolarizing and hyperpolarizing voltage steps are clearly demonstrated (see Fig. 12) when the combined data from Figs. 6, 7, and 9 are presented in the form of a linearized Boltzmann plot using the method of Keynes and Rojas (1974, 1976). In Fig. 12, since both ordinate and abscissa have equivalent units, the slope of the lines through the plotted data points should directly indicate the effective valence of each distribution. The 60-mV parallel shift between curves *d* and *f*, associated with voltage-insensitive charge equilibration during prolonged depolarizing pulses, is very clear here (see also Fig. 6). The isochronal data, for depolarizing prepulses of 1 ms or shorter (curves *a–c*), might have been better fit by an asymptotic approach such as we used for the voltage-sensitive component of hyperpolarization-induced charge movement (see Appendix). Nevertheless the changes in slope, which appear for both depolarizing (*a–c*) and hyperpolarizing steps (*g–i*) while voltage-sensitive charge movement is occurring, are readily apparent. Can these lower slopes provide a valid indicator of effective particle valence?

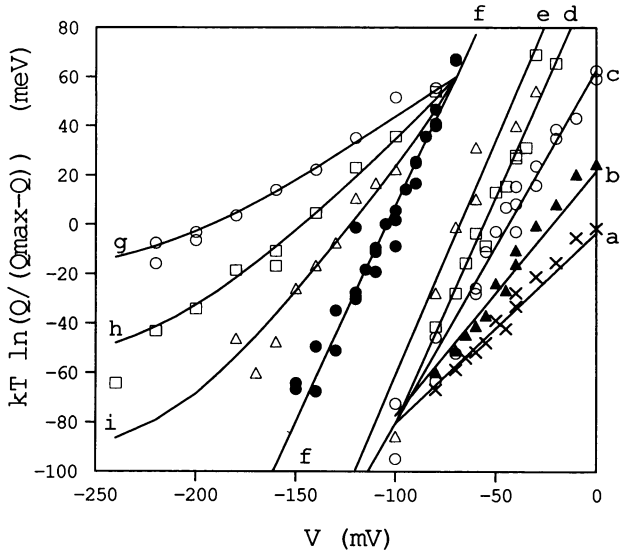

FIGURE 12 Differences in slope between Q-V_{dep} curves obtained from −140 mV holding potential (curves *a–e*) and Q-V_{hyp} curves from −70 mV holding potential (curves *g*, *h*, and *i*) are accentuated when the data are presented according to the linearized Boltzmann plot introduced by Keynes and Rojas (1974). The equilibrium Q-V_h distribution is shown as curve *f*. Combined data from Figs. 6, 7, and 9 are presented here, together with lines of fit generated as indicated in the legends for those figures. (Data symbols are those used in the original figures.)

A crucial assumption underlying the Boltzmann relationship is that the system must be studied under equilibrium conditions. We have been careful to demonstrate that this assumption is valid for the experimental conditions of the Q-V_h curve (see Fig. 4). However, we have also shown that voltage-sensitive charge movement is completed within 2 ms during depolarizing pulses (Fig. 7). Thus, although the component of the Q-V curve obtained using depolarizing pulses may reflect the behavior of the system when it is far from equilibrium, a quasi–steady state has been established (at all times longer than 2 ms) with respect to voltage-sensitive movement of the gating particles. It therefore seems reasonable that such curves should show the same effective valence as the equilibrium Q-V_h curve (see Figs. 6 and 7). By contrast no such quasi–steady state can be demonstrated during hyperpolarization-induced gating charge movements; return of charge during hyperpolarizing pulses remains voltage sensitive throughout the entire recovery process (Fig. 9). In the absence of any quasi–steady state comparable to that found for Q-V_{dep}, the Boltzmann analysis cannot be applied to hyperpolarization-induced charge movements. Hence the slope of the Q-V_{hyp} component within a complex Q-V curve should not be used as an indicator of particle valence. Both the Almers (1978) and Keynes (1986) interpretations of the low slope region of the Q-V curve can therefore be rejected.

Towards a model for the sodium channel gating current generator

The similarity of the slopes of the Q-V_{dep} and Q-V_h distributions (see Fig. 6) places sharp constraints on the class of models introduced by Armstrong and Bezanilla (1977), in which the full valence of sodium channel activation is build up within a linear sequence of preopen transitions leading to a final channel opening step (see also Armstrong and Gilly, 1979; Fohlmeister and Adelman, 1985). First, if the full channel valence is 4 to 6*e* (see Keynes and Rojas, 1976; Armstrong and Bezanilla, 1977; Almers, 1978; Vandenberg and Horn, 1984) then a gating particle valence of 1.9*e* indicates that two or more non-interacting gating particles must be associated with each sodium channel. Second, the excellent fit to a single Boltzmann distribution seen in our Q-V_h curves suggests that gating particles are uniform and distribute between no more than two equilibrium particle positions (which must be separated by the full 1.9*e*). After all, if intermediate states showed appreciable equilibrium occupancy, part of the gating current (observed in a step to test potential from any nonsaturated holding potential) would necessarily be generated across transitions of reduced total valence. Those lower valence transitions would inevi-

tably distort the Q-V_h curve. Since no such distortions are apparent in our data, we conclude that the same two states must be involved at all holding potentials and occupancy of any intermediate states must always be negligible at equilibrium. But the Q-V_{dep} curve also shows a single $1.9e$ valence at all potentials. Thus the quasi–steady state achieved at the end of the voltage-sensitive component of gating particle movement must also involve negligible occupancy of intermediate states. Thus, across a wide range of voltages, the rate constants governing any such intermediate states must be such as to leave negligible state occupancies at times longer than 2 ms (just as occupancy of the open state is also very low under similar conditions).

In further support of this conclusion, the slopes of Q-V_{dep} curves seem to be independent of holding potential. We have noted a mean slope of $1.79e \pm 0.15$ (SD) from six experiments with holding potentials of -140 or -120 mV, as compared with a slope of $1.70e \pm 0.22$ (SD) from three experiments from -100 mV holding potential. Thus reacting gating particles seem to pass through the same fraction of the applied field during any depolarization-induced conformational change, regardless of holding potential or final potential. It follows that all Q-V_{dep} curves should have the same "shape" regardless of the holding potential from which they are generated. (Although the midpoint [V_o] may change depending on the integration period or prepulse duration used.) When this hypothesis is stated in quantitative form (see Appendix), it provides an acceptable fit to the data of Fig. 10 where it was used to generate the smooth curves through our experimental data points for depolarizing test pulses.

We have seen that hyperpolarization-induced charge movements violate the assumptions of the Boltzmann approach. Nevertheless, if only two gating particle positions are heavily occupied at equilibrium then those gating particles which are in their depolarization-favored position may also be expected to cross the same fraction of the applied field during any hyperpolarization-induced charge movement. Thus all Q-V_{hyp} curves (for given prepulse duration or integration period) should have the same "shape" regardless of holding potential. Again the quantitative expression of this hypothesis (see Appendix) has proved useful in describing experimental data, generating the smooth curves through the Q-V_{hyp} data points shown in Figs. 9, 10, and 12.

Following such substantial evidence that gating particles constitute a single uniform population, the 60 mV shift between the Q-V_{dep} and Q-V_h slopes takes on added significance. Additionally we have seen that those gating charges which cross in the first 100 μs have a midpoint of around 0 mV. The full shift in voltage sensitivity during, for example a 2-min depolarizing voltage step, is thus 100 mV. The simplest explanation for the existence of such large voltage offsets within a uniform particle population is that they are caused by localized bias potentials applied across the gating particles. Such biasing could arise from coulombic forces generated by nonspecific dipole movements adjacent to the channel, by nonspecific conformational changes within the channel molecule, or by conformational changes specifically associated with channel gating. Regardless of which of these mechanisms is involved, the slowly changing voltage reactivity of the particles during prolonged depolarization would then be perceived as gating charge "immobilization" (Bezanilla et al., 1982). But if these biasing charge movements involved any significant motion in the direction of the transmembrane potential field, then they would necessarily contribute to the Q-V_h valence (although not the Q-V valence). Our results set a maximum value on the net effective valence of all such biasing charges, from the sum of the standard errors in the slopes of the Q-V_h and Q-V_{dep} distributions, of less than $\sim 0.15e$.

Thus our data support a general kinetic model in which a single uniform population of voltage-sensitive gating particles is coupled by coulombic forces to one or more voltage-insensitive "immobilizing" particles. However, neither the number of the immobilizing particles nor the detailed nature of the supposed electrostatic interactions can be uniquely specified at this time.

The four-state and eight-state models introduced by Bezanilla et al. (1982) are both specific instances within this general model class, although in both models the supposed sequences of preopen states has been collapsed into a single transition. This simplification seems entirely appropriate in modeling steady-state properties, in view of the low final occupancy of the intermediate states within this reaction sequence. Second, very specific assumptions were made with respect to the physical nature of both the biasing and gating particles. The four-state model presumes that a negatively charged gating particle is biased by interaction with a positively charged slow inactivation gate located near the outside surface of the sodium channel. In the form utilized by Fernandez et al. (1982), the four-state model gives a midpoint of -27 mV for the unbiased gating particles and a midpoint of -77 mV for these particles when biased by interaction with the slow inactivation gate. The more complex eight-state model includes an additional fast inactivation gate which also interacts with the gating particle. The fast inactivation gate is presumed to be a positive particle located on the inside surface of the membrane. Two biasing particles generate four interactive conditions for the gating particles, with midpoints for these distributions being $+22$ mV, -23 mV, -38 mV, and -83 mV for the model parameters quoted by Bezanilla et al. (1982). Despite the success of these models in simulations of gating current data, the identification of

charge immobilization with sodium channel inactivation may be premature.

Following the initial work of Bezanilla and Armstrong (1977), further evidence in favor of activation-inactivation coupling has been provided by Goldman and Kenyon (1982) from macroscopic currents, as well as single channel studies by Aldrich and Stevens (1984). However, sodium channels may inactivate without first opening (Horn et al., 1981) and the hypothesized coupling to inactivation must occur to preopen states as well as to the open state (Horn and Vandenberg, 1984). Similarly, Vandenberg and Horn (1984) failed to find a statistical advantage for coupled models in predicting single channel kinetics and concluded that the initial inactivation step may be independently voltage sensitive. Nevertheless the evidence remains overwhelming that the gating particles must be sequentially coupled to subsequent immobilization processes (see reviews by Armstrong, 1981; Bezanilla, 1982; French and Horn, 1983; Hille, 1984). We have therefore preferred to identify the biasing particles only with the charge immobilizing processes, without specifying the role which these particles may play in the gating of ion channels. Our data (see Fig. 11 *B*), as well as that of Bezanilla et al. (1982), show that gating current recovers from long term inactivation more rapidly than does I_{Na}, strongly suggesting that recovery from "slow immobilization" and recovery from "slow inactivation" are not identical processes.

We have carried out preliminary testing of several additional models which fall into the general class described above. At least two biasing particles are required to approach the kinetic complexity of the experimentally observed charge equilibration processes. An alternative eight-state model, in which a positive gating particle is attracted to a negatively charged "slow immobilization" particle near the outside of the channel and repelled by a positively charged "fast immobilization" particle near the inside of the channel, has shown interesting possibilities. Nevertheless we shall demonstrate the general behavior of this class of models using the more familiar Bezanilla et al. (1982) eight-state formulation, without modification of the terminology they introduced.

Finally, we must consider the constraint provided by the asymmetry between responses to depolarizing and hyperpolarizing pulses which has been so noticeable in our data. Since gating charge immobilization was first described by Armstrong and Bezanilla (1977), it is clear that the gating particles can demonstrate markedly asymmetric behavior in ON and OFF voltage steps under certain conditions. Thus gating particles in their depolarization-favored position may be partially (or fully) immobilized, so that they return across the membrane with the relatively slow rates characteristic of recovery from the immobilized state. This interpretation seems consistent with the slow component of charge return seen at −180 and −200 mV in Fig. 11 *A*. An alternative possibility could be that the asymmetries observed here might arise from non-Markovian behavior of the channel control mechanism (see, for example, Patlak and Ortiz, 1985). On the other hand our symmetrical equilibrium Q-V_h distribution seem fully consistent with a Markovian mechanism. We demonstrate below that asymmetric behavior, apparently equivalent to that seen in our data, can be generated by charge immobilization within the eight-state Bezanilla model.

Simulations of experimental data

The eight-state model explored here (see Fig. 13) has been adapted from the squid axon formulation presented by Bezanilla et al. (1982). Small changes were made in model parameters (see Table 1) so as to approximate the quantitative differences between the steady-state properties of crayfish and squid axons noted above. We have previously reported that gating currents in crayfish are some threefold faster than in squid axons at comparable temperatures (Starkus et al., 1981), so the energy barrier

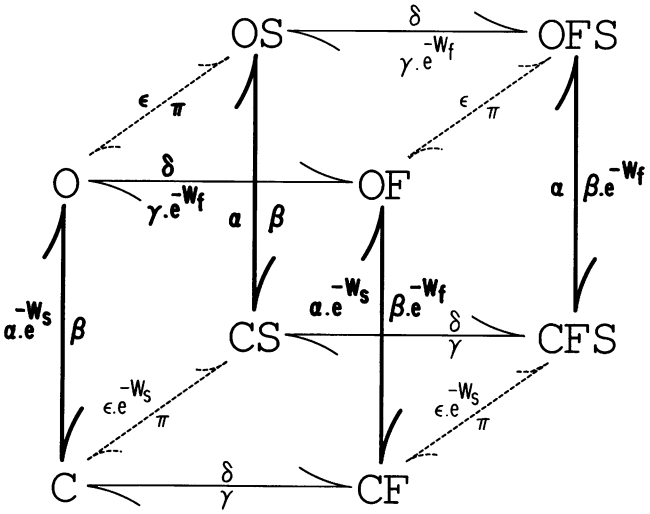

FIGURE 13 Cartoon of the eight-state model used for the data simulations shown in Fig. 14. Redrawn from Bezanilla et al. (1982) without changes in the symbols used for conformational states or rate constants. Transitions involving movement of the gating particle are indicated by vertical arrows. Transitions involving movement of the fast immobilizing charge are shown by horizontal arrows, while angled arrows (*dashed*) indicate transitions associated with movement of the slow immobilizing charge. Rates for all transitions are affected, as indicated, by the form of the interactions assumed between the gating particles and the immobilizing charges (see text). For all states labeled *O* the gating particle is in its "open," or depolarization-favored, position. For states labeled *C* the gating particle is in its "closed," or hyperpolarization-favored, position. States labeled *F* and/or *S* are fast and/or slow immobilized.

TABLE 1. Parameters used for the eight-state model shown in Fig. 13 (terminology follows that used by Bezanilla et al., 1982)

	Voltage-sensitive transitions			Gate–particle interaction energies		Voltage-insensitive transitions			
	W_1	W_2	z	W_f	W_s	γ	δ	ϵ	π
Squid	20.55	22.09	1.6	4	3	0.0075	0.0015	5.5e-8	1.0e-8
Crayfish	17.3	22.3	1.8	8	4	0.08	0.003	7.0e-6	2.0e-6

Voltage-sensitive rate constants were calculated from the equations shown by Bezanilla et al. (1982), in which:

$$\text{alpha} = (kT/h) \cdot \exp - [W_1 - (ezV/2kT)] \text{ and beta} = (kT/h) \cdot \exp - [W_2 + (ezV/2kT)],$$

where W refers to the difference in kT units from the well to the barrier peak and the other symbols have their usual significance. The voltage-insensitive rate constants are given in reciprocal microseconds.

(W_1) was lowered to approximate crayfish axon kinetics. Thereafter the model was adjusted to fit our steady-state data using the following method.

Step 1: We adjusted the interaction energies (W_s and W_f) to produce the increased spread in V_0 values required by the greater voltage shifts between Q-V_{dep} and Q-V_{hyp} distributions in crayfish axons. (V_0 values for each of the four voltage-sensitive transitions can be readily calculated remembering that forward and back reaction rates are equal where $V = V_0$.) The principal change required to adapt the eight-state model to crayfish axons (see Table 1) was a doubling of the interaction energy between the fast inactivation gate and the gating particle.

Step 2: We then adjusted the voltage-insensitive reaction rates to better approximate the relative "weightings" for each voltage-sensitive transition within the "mean" behavior exposed by simulations of the experimental measures: Q-V_h, Q-V_{dep}, and Q-V_{hyp}. The principal change required here was a 10-fold increase in the rate constant gamma. This change maintains a reasonably fast immobilization rate while providing for the rapid kinetics out of the CFS state noted below.

Step 3: The final step involved iteration of steps 1 and 2 above until an acceptable fit to crayfish axon data was achieved. Thereafter all simulations were carried out by standard iterative procedures. Simulated pulse protocols were identical to those employed for our axon data; simulated gating currents obtained from these pulse protocols were analyzed by the same methods used for experimental data.

As shown in Fig. 14 *A*, the behavior of this eight-state model seems almost identical to the experimental data presented in Fig. 10, except that the model axon recovers rather more rapidly than our crayfish axons at negative potentials. There can be no doubt that for this model, as for the axon, the Q-V_{dep} curve parallels the Q-V_h relationship (see Fig. 14 *A*) when full voltage-sensitive charge movement is collected. However for short (100 μs) prepulse durations (Fig. 14 *B*, *crosses*) the midpoint moves to the right of the Q-V_{dep} curve obtained using 2-ms prepulses (*solid triangles*) and the apparent valence is reduced. Similarly Q-V_{hyp} curves show a reduced valence which increases as a function of the intregration period (Fig. 14 *B*). Thus these simulations clearly demonstrate an apparent asymmetry between responses to depolarizing and hyperpolarizing voltage steps similar to that seen in the axon data, while also duplicating the effect of holding potential on the "shape" of the Q-V curve.

The mechanism underlying the asymmetry seen in Fig. 14 *B* is as follows. Only three states in this model ever show >5% equilibrium occupancy. State C (see Fig. 13) is the only state with high equilibrium occupancy when the gating particles are in their hyperpolarization-favored position. However states OF and OFS both show substantial equilibrium occupancy at depolarized holding potentials. Thus a hyperpolarizing step from a depolarized holding potential involves a net flux from states OF and OFS into state C. But the voltage-sensitive reactions leading out of states OFS and OF have midpoints of −174 and −120 mV, respectively. For comparison the midpoint for OS-CS is −67 mV and for the O-C transition is −13 mV. Even at a test potential of −240 mV, charge returns through pathways other than the relatively slow OF-CF and OFS-CFS transitions, thereby exposing eigenvalues which are markedly affected by the voltage insensitive, charge immobilizing, reactions. Hence the long maintained voltage sensitivity of the charge return process. By contrast the rates of re-equilibration amongst the "closed" states are relatively fast, such that returning charge rapidly re-enters the equilibrium state (C) which is favored under hyperpolarized conditions. Thus even during exact simulations of the Fig. 11 protocols, no changes are seen in the voltage sensitivity of depolarization-induced charge movements.

In conclusion, our simulation studies have shown that the steady-state properties of sodium channel gating

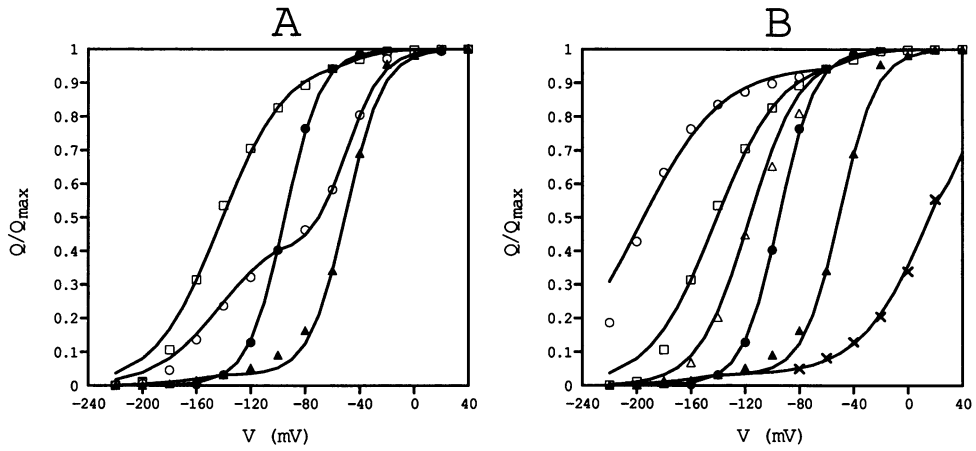

FIGURE 14 Simulations of experimental data obtained using the eight-state model introduced by Bezanilla et al. (1982), see Fig. 13. (*A*) Q-V curves change their shape with change of holding potential. As in our data, the fraction of charge moving with low apparent slope increases as holding potential is moved in the depolarizing direction. Three simulated Q-V curves are shown from holding potentials of −140 mV (*solid triangles*), −100 mV (*open circles*), and −60 mV (*open squares*). Also shown is an equilibrium Q-V_h simulation (*solid circles*). (*B*) Q-V curves change slope as voltage-sensitive charge movement occurs. There is a marked asymmetry in the duration of voltage-sensitive charge movement in depolarizing versus hyperpolarizing pulses. Two simulated Q-V_{dep} curves are shown for depolarizing prepulse durations of 0.1 ms (*crosses*) and 2 ms (*solid triangles*). Three simulated Q-V_{hyp} curves are shown for hyperpolarizing prepulse durations of 1 ms (*open circles*), 6 ms (*open squares*), and 100 ms (*open triangles*). Simulated Q-V_h data (*solid circles*) is also included. Parameters of fit for the smooth curves drawn through the simulated data are tabulated below.

	Panel *A*						Panels *A* and *B*	Panel *B*				
	Q-V_{dep}			Q-V_{hyp}			Q-V_h	Q-V_{dep}		Q-V_{hyp}		
V_h	−60	−100	−140	−60	−100	−140	−160 to −40	−140	−140	−60	−60	−60 mV
t	—	—	—	6	6	6	—	2	0.1	1	6	100
V_0	−50	−50	−50	−142	−142	−142	−95	−50	19	−198	−142	−117 mV
z	1.8	1.8	1.8	1.0	1.0	1.0	1.8	1.8	0.93	0.8	1.0	1.3*e*
s_∞	0.91	0.39	0.03	0	0	0	—	0.03	0.03	0	0	0
q_h	0.94	0.40	0.03	0.94	0.40	0.03	—	0.03	0.03	0.94	0.94	0.94

t, prepulse duration (ms). All other symbols are defined in the Appendix.

currents may be generated by a strictly Markovian channel mechanism, provided that this mechanism contains the features of the "general model" introduced here, namely: (*a*) a uniform population of voltage-sensitive gating particles which are coulombically coupled to (*b*) at least two biasing particles constrained to move only in a plane perpendicular to the applied membrane field.

Nevertheless, the close correspondence between both crayfish and squid axon steady-state data and the behavior of appropriately fitted eight-state Bezanilla models, does not necessarily support the specific set of assumptions made by Bezanilla et al. (1982) concerning the physical nature of the gating (I_g-generating) and biasing (or charge-immobilizing) particles. Further work will be required to evaluate the relative performance of their assumptions, versus other possible interaction mechanisms consistent with this general model class, before any such conclusions can be drawn.

APPENDIX

Fitting Q-V data points obtained from nonsaturated holding potentials

The Q-V_{dep} distribution

Definitions and Assumptions: We shall first describe the various gating charge distributions by separate variable names: q_h will be used for points on any Q-V_h curve, p describes the Q-V_{dep} curve from a negative saturated holding potential (e.g., from −140 mV), and s defines the scaled Q-V_{dep} curve obtained from any nonsaturated holding potential (see Discussion). The limiting values of the s-V distribution are s_∞ at its

hyperpolarizing end and s_{max}, which defines the total depolarizing charge movement within this scaled distribution. This s-V curve crosses the Q-V_h curve at s_h, the value of s at holding potential. Finally we retain the variable q to describe smooth curves drawn through experimental data points. Our purpose is thus to calculate q-V distributions, using the minimum number of external assumptions. Where q_h has been determined experimentally as Q/Q_{max} at the given holding potential and assuming the p-V distribution is describable by a simple Boltzmann equation for which the variables z and V_0 have already been obtained, then values of q may be calculated as follows.

Procedure: The first step is to calculate p_h, the value of p at holding potential, from the Boltzmann equation:

$$p = 1/\{1 - \exp[-z(V - V_0)/kT]\}, \quad (1)$$

where the s-V distribution has the same "shape" as the p-V curve, then the ratio $p_h/(1 - p_h)$ must be equal to the ratio $s_h/(1 - q_h)$.Thus:

$$s_h = (p_h - q_h \cdot p_h)/(1 - p_h). \quad (2)$$

Since all available mobile charge can be collected within normal integration periods at positive test potentials, s_{max}, is

$$s_{max} = (1 - q_h) + s_h, \quad (3)$$

while s_s, the minimum steady-state level of the s-V distribution, must be

$$s_s = q_h - s_h. \quad (4)$$

When values of p for any depolarized potential V are calculated from Eq. 1, then it follows that

$$q = p \cdot s_{max} + s_s. \quad (5)$$

Eq. 5 was used to generate the smooth curves through the Q-V_{dep} data of Fig. 10 and the simulated data points of Fig. 14, *A* and *B*.

The Q-V_{hyp} distribution

Definitions and Assumptions: We recognize (see Discussion) that hyperpolarization-induced charge movements do not fulfill the equilibrium condition required for application of a Boltzmann analysis. However the Boltzmann approach remains a useful description of the form of our data. The same three analytical distributions, q_h-V_h, p-V, and s-V may therefore be used to describe hyperpolarization-induced charge movements provided that no theoretical significance is applied to the slope factor, z. Note that p-V is now the Q-V_{hyp} curve, for defined prepulse duration or integration period, from a depolarized saturated holding potential. There is an additional problem in describing Q-V_{hyp} curves, however, since charge immobilization is not completely reversed, within reasonable integration periods, even at very negative test potentials. Our approach has been to first characterize an idealized p-V distribution, for the required prepulse duration or integration period by applying a linear regression to data sets obtained using the same prepulse duration or integration period, but from a strongly depolarized holding potential (such as the linearized data points of Fig. 12, lines *e–g*). The variables z and V_0 are obtained for the idealized p distribution from this regression equation. Q-V_{hyp} curves can now be calculated for any intermediate unsaturated holding potential for which q_h has been determined experimentally, according to the following procedure.

Procedure: The first step is to obtain s_s, the fraction of unrecovered charge under the conditions of the experiment in question, by direct examination of the experimental data at the most negative potentials available. Thereafter, by definition

$$s_h = q_h - s_s, \quad (6)$$

while the equivalent ratios for the p and s distributions, $p_h/(1 - p_h)$ and in this case $s_h/(s_{max} - s_h)$, can be rearranged to solve for s_{max} in terms of known parameters:

$$s_{max} = (s_h - p_h \cdot s_h)/p_h + s_h. \quad (7)$$

Then, just as for the depolarization-induced charge movements, values of q can be calculated for any hyperpolarized potential from Eq. 5, where p has been obtained from Eq. 1 using the appropriate values of z and V_0 for the idealized p distribution. Q-V_{hyp} curves calculated by this method have been included in Figs. 9, 10, 14, *A* and *B*.

We thank Dr. Steven Heggeness, Richard Foulk, and Nicolas Rayner for their help in development of the modeling programs used here, as well as Daniel Alicata and Sarah Fishman for their technical assistance to this project. We also thank Dr. Peter Ruben for his many helpful comments during the preparation of this manuscript.

This work was supported by the National Institutes of Health (NIH) through research grant S21151-04 (to J. G. Starkus), with additional support from the NIH RCMI grant RR-03061, the Hawaii Heart Association, the University of Hawaii Research Council, and BRSG 2S07 RR07026 awarded by the Biomedical Research Support Grant Program, Division of Research Resources, National Institutes of Health.

Received for publication 24 February 1988 and in final form 5 September 1988.

REFERENCES

Aldrich, R. W., and C. F. Stevens. 1984. Inactivation of open and closed sodium channels determined separately. *Cold Spring Harbor Symp. Quant. Biol.* 48:147–154.

Almers, W. 1978. Gating currents and charge movements in excitable membranes. *Rev. Physiol. Biochem. Pharmacol.* 82:6–190.

Armstrong, C. M. 1981. Sodium channels and gating currents. *Physiol. Rev.* 61:644–683.

Armstrong, C. M., and F. Bezanilla. 1974. Charge movement associated with the opening and closing of the activation gates of the Na channels. *J. Gen. Physiol.* 63:533–552.

Armstrong, C. M., and F. Bezanilla. 1977. Inactivation of the sodium channel. II. Gating current experiments. *J. Gen. Physiol.* 70:567–590.

Armstrong, C. M., and W. F. Gilly. 1979. Fast and slow steps in the activation of sodium channels. *J. Gen. Physiol.* 74:691–711.

Bezanilla, F. 1982. Gating charge movements and kinetics of excitable membrane proteins. *In* Proteins of the Nervous System: Structure and Function. B. Haber, J. R. Perez-Polo, and J. D. Coulter, editors. Alan R. Liss, Inc., New York. 3–16.

Bezanilla, F., and C. M. Armstrong. 1975. Properties of the sodium channel gating current. *Cold Spring Harbor Symp. Quant. Biol.* 40:297–304.

Bezanilla, F., and C. M. Armstrong. 1977. Inactivation of the sodium channel. I. Sodium current experiments. *J. Gen. Physiol.* 70:549–566.

Bezanilla, F., R. E. Taylor, and J. M. Fernandez. 1982. Distribution and kinetics of membrane dielectric polarization. I. Long-term inactivation of gating currents. *J. Gen. Physiol.* 79:21–40.

Fernandez, J. M., F. Bezanilla, and R. E. Taylor. 1982. Distribution and

kinetics of membrane dielectric polarization. II. Frequency domain studies of gating currents. *J. Gen. Physiol.* 79:41–67.

Fohlmeister, J. F., and W. J. Adelman. 1985. Gating current harmonics. II. Model simulations of axonal gating currents. *Biophys. J.* 48:391–400.

French, R. J., and R. Horn. 1983. Sodium channel gating: models, mimics, and modifiers. *Annu. Rev. Biophys. Bioeng.* 12:319–356.

Goldman, L., and J. L. Kenyon. 1982. Delays in inactivation development and activation kinetics in *Myxicola* giant axons. *J. Gen. Physiol.* 80:83–102.

Heggeness, S. T., and J. G. Starkus. 1986. Saxitoxin and tetrodotoxin. Electrostatic effects on sodium channel gating current in crayfish axons. *Biophys. J.* 49:629–643.

Hille, B. 1984. Ionic Channels of Excitable Membranes. Sinauer Associates, Inc., Sunderland, MA.

Horn, R., and C. A. Vandenberg. 1984. Statistical properties of single sodium channels. *J. Gen. Physiol.* 84:505–534.

Horn, R., J. Patlak, and C. Stevens. 1981. Sodium channels need not open before they inactivate. *Nature (Lond.).* 291:426–427.

Keynes, R. D. 1986. Properties of the sodium gating current in the squid giant axon: tetrodotoxin saxitoxin and the molecular biology of the sodium channel. *Ann. NY Acad. Sci.* 479:431–438.

Keynes, R. D., and E. Rojas. 1974. Kinetics and steady state properties of the charged system controlling sodium conductance in the squid giant axon. *J. Physiol. (Lond.).* 239:393–434.

Keynes, R. D., and E. Rojas. 1976. The temporal and steady state relationships between activation of the sodium conductance and movement of the gating particles in the squid giant axon. *J. Physiol. (Lond.).* 255:157–189.

Meves, H. 1974. The effect of holding potential on the asymmetry currents in squid giant axons. *J. Physiol. (Lond.).* 243:847–867.

Patlak, J. B., and M. Ortiz. 1985. Slow currents through single sodium channels of the adult rat heart. *J. Gen. Physiol.* 86:89–104.

Rayner, M. D., and J. G. Starkus. 1988. Holding potential affects the shape of the Q-V curve in crayfish giant axons. *Biophys. J.* 53:17a. (Abstr.)

Shrager, P. 1974. Ionic conductance changes in voltage clamped crayfish axons at low pH. *J. Gen. Physiol.* 64:666–690.

Starkus, J. G., and M. D. Rayner. 1988. Changes in holding potential demonstrate a symmetrical steady state charge distribution in crayfish axons. *Biophys. J.* 53:17a. (Abstr.)

Starkus, J. G., and P. Shrager. 1978. Modification of slow sodium inactivation in nerve after internal perfusion with trypsin. *Am. J. Physiol.* 4:C238–244.

Starkus, J. G., B. D. Fellmeth, and M. D. Rayner. 1981. Gating currents in the intact crayfish giant axon. *Biophys. J.* 35:521–533.

Starkus, J. G., S. T. Heggeness, and M. D. Rayner. 1984. Kinetic analysis of sodium channel block by internal methylene blue in pronased crayfish giant axons. *Biophys. J.* 46:205–218.

Vandenberg, C. A., and R. Horn. 1984. Inactivation viewed through single sodium channels. *J. Gen. Physiol.* 84:535–564.